HHS Public Access

Author manuscript

Dev Cell. Author manuscript; available in PMC 2021 May 12.

Published in final edited form as:

Dev Cell. 2009 January ; 16(1): 70–82. doi:10.1016/j.devcel.2008.12.009.

Nrarp Coordinates Endothelial Notch and Wnt Signaling to Control Vessel Density in Angiogenesis

Li-Kun Phng[1], **Michael Potente**[2], **Jonathan D. Leslie**[3], **Jane Babbage**[1], **Daniel Nyqvist**[4], **Ivan Lobov**[5], **Jennifer K. Ondr**[6], **Sujata Rao**[6], **Richard A. Lang**[6], **Gavin Thurston**[5], **Holger Gerhardt**[1,*]

[1]Vascular Biology Laboratory, London Research Institute – Cancer Research UK, 44 Lincoln's Inn Fields, WC2A 3PX London, UK

[2]Institute for Cardiovascular Regeneration, Centre of Molecular Medicine & Department of Cardiology, Internal Medicine III, Goethe University, Theodor-Stern-Kai 7, D-60590 Frankfurt (Main), Germany

[3]Vertebrate Development Laboratory, London Research Institute – Cancer Research UK, 44 Lincoln's Inn Fields, WC2A 3PX London, UK

[4]Vascular Biology Group, IFOM, The FIRC Institute for Molecular Oncology, Via Adamello 16, 20139 Milan, Italy

[5]Regeneron Pharmaceuticals, Inc., 777 Old Saw Mill River Road, Tarrytown, NY 10591, USA

[6]Department of Ophthalmology and Division of Developmental Biology, Children's Hospital Research Foundation, 3333 Burnet Avenue, Cincinnati, OH 45229, USA

SUMMARY

When and where to make or break new blood vessel connections is the key to understanding guided vascular patterning. VEGF-A stimulation and Dll4/Notch signaling cooperatively control the number of new connections by regulating endothelial tip cell formation. Here, we show that the *Notch-regulated ankyrin repeat protein* (*Nrarp)* acts as a molecular link between Notch- and Lef1-dependent Wnt signaling in endothelial cells to control stability of new vessel connections in mouse and zebrafish. Dll4/Notch-induced expression of *Nrarp* limits Notch signaling and promotes Wnt/Ctnnb1 signaling in endothelial stalk cells through interactions with Lef1. BATgal-reporter expression confirms Wnt signaling activity in endothelial stalk cells. Ex vivo, combined Wnt3a and Dll4 stimulation of endothelial cells enhances Wnt-reporter activity, which is abrogated by loss of *Nrarp*. In vivo, loss of *Nrarp*, *Lef1*, or endothelial *Ctnnb1* causes vessel regression. We suggest that the balance between Notch and Wnt signaling determines whether to make or break new vessel connections.

*Correspondence: holger.gerhardt@cancer.org.uk.

SUPPLEMENTAL DATA

Supplemental Data include Supplemental Experimental Procedures, twelve figures, and three movies can be found with this article online at http://www.cell.com/developmental-cell/supplemental/S1534-5807(08)00519-4/.

INTRODUCTION

Formation of a vascular network during sprouting angiogenesis is controlled by coordinated endothelial cell (EC) migration, proliferation, and differentiation. Tubular sprouting from epithelial/endothelial structures or cell clusters in *Drosophila* and vertebrates relies on a set of conserved basic principles including (1) induction and selection of a leading tip cell, (2) sprout elongation and stalk formation through intercalation and/or proliferation, (3) branching, (4) anastomosis and, finally, (5) stabilization of the connected network (Lubarsky and Krasnow, 2003). In the vertebrate vasculature, sprouting is induced by local production of proangiogenic factors, including vascular endothelial growth factor A (VEGF-A). Endothelial VEGF receptor 2 (VEGFR2) stimulation and signaling is required for filopodia formation and tip cell induction and is also involved in stalk cell proliferation (Gerhardt et al., 2003). Recent work in mouse and zebrafish illustrates that VEGF-A/VEGFR2-dependent signaling also induces expression of the Notch receptor ligand Delta-like 4 (Dll4) in endothelial tip cells (Leslie et al., 2007; Liu et al., 2003; Lobov et al., 2007). Dll4 signals in a contact-dependent manner to neighboring endothelial cells through Notch1 to limit their tip cell behavior (Hellstrom et al., 2007b; Leslie et al., 2007; Lobov et al., 2007; Siekmann and Lawson, 2007; Suchting et al., 2007). This mechanism regulates and balances the number of tip cells required for effective sprouting and network formation.

Subsequent to sprouting angiogenesis, the mature hierarchical tubular network is a result of extensive pruning of the initial primitive plexus through selective branch regression. With the exception of hyaloid vessel regression (Lobov et al., 2005; Rao et al., 2007), the detailed mechanism of vascular pruning is poorly understood. Inhibition of VEGF-A signaling in adult mice leads to vessel regression associated with lumenal fibrin clot formation, EC apoptosis, formation of empty basement membrane sleeves, and pericyte migration to remaining patent vessels (Baffert et al., 2006). Loss or ectopic activation of endothelial Notch signaling increases or reduces vascular density, respectively, indicating that endothelial Notch signaling is a key regulator of vascular density (Gridley, 2007). The downstream targets of endothelial Notch signaling in this process remain unknown.

The *Notch-regulated ankyrin repeat protein* (*Nrarp*) is induced by Notch signaling through the CSL-dependent pathway (Krebs et al., 2001; Lamar et al., 2001; Pirot et al., 2004). In the mouse, the *Nrarp* gene encodes a small protein of 114 amino acids with two ankyrin repeat domains. In the zebrafish, two *nrarp* paralogs, *nrarp-a* and *nrarp-b*, encode proteins of 112 and 111 amino acids, respectively (Topczewska et al., 2003), which share 80% amino acid sequence homology with mouse Nrarp (Topczewska et al., 2003). By investigating the expression and function of murine *Nrarp* and zebrafish *nrarp-a* and *nrarp-b* in angiogenesis, we find that Nrarp acts downstream of Notch at newly formed branch points to regulate vascular density. Nrarp performs this function by integrating endothelial Notch and Wnt signaling to control stalk cell proliferation and to stabilize new endothelial connections during angiogenesis.

RESULTS

Nrarp Is an Endothelial Target of Notch Signaling during Angiogenesis

In mouse E10.5 embryos, *Nrarp* is prominently expressed in the central nervous system and in the presomitic mesoderm, as reported previously (Krebs et al., 2001). In addition, *Nrarp* is expressed in intersomitic vessels (Figure 1A) and in vessels of the limb buds (Figure 1B). Counterstaining of blood vessels with Endomucin indicated the strongest signal at vascular branch points (Figures 1B and 1C).

In the early postnatal mouse retina, *Nrarp* expression is prominent in ECs at the migrating front of the vasculature. Strongest expression is detected behind the leading tip cells (Figure 1D). The distribution of *Nrarp* expression coincides with regions of high Notch activity, as revealed previously in the transgenic Notch reporter mouse (TNR1) and the nuclear localization of Notch intracellular domain (NICD) (Hellstrom et al., 2007b). Close observation of *Nrarp* expression in 200 Isolectin-B4-labeled sprouts in 3 P5 retinas revealed *Nrarp* mRNA in only 7% ± 2 of the leading tip cells. For comparison, 84% ± 10 of the tip cells were positive for *Dll4* mRNA, consistent with the idea that tip cells signal through Dll4 to induce Notch signaling, and hence *Nrarp* expression, in stalk cells. *Nrarp* is also prominently expressed in some ECs of the newly formed plexus.

To determine whether the endothelial expression of *Nrarp* in the retina is regulated by Notch signaling, we suppressed Notch signaling by treating early postnatal mice with the γ secretase inhibitor (GSI) DAPT, and with human Dll4-Fc. Six hours post-treatment with DAPT, *Nrarp* mRNA was decreased significantly in ECs by whole-mount in situ hybridization (Figure 1E) and reduced by over 70% by qPCR analysis of whole retina lysates (Figure 1F). Also, 24 hr post-treatment with human Dll4-Fc, *Nrarp* mRNA levels were significantly reduced (Figure 1F). Primary human endothelial cells (HUVECs) plated on Dll4-coated dishes upregulated *NRARP*, as well as the known Notch targets *HEY1* and *HEY2* (Figure 1G). Together, these data illustrate that Dll4-Notch signaling positively regulates *Nrarp* expression in ECs.

In the zebrafish, the two paralogs *nrarp-a* and *nrarp-b* are abundant in the neural tube and in the presomitic mesoderm (Figures 1H and 1J; see Figure S1 available online). In addition, we observed *nrarp-a* in the dorsal aorta (DA) at 24 hr post-fertilization (hpf) (Figures 1H and 1J). At higher magnification, *nrarp-a* expression is also detected in some ECs of the intersegmental vessels (Figure 1I), but appears absent from the cardinal vein.

Defects in Retinal Vessel Migration, Density, and Morphology in *Nrarp*-Deficient Mice

We generated *Nrarp*-deficient mice by replacing the genomic coding region of *Nrarp* with a *LacZ* reporter gene (Figure S2) using Velocimouse technology (Valenzuela et al., 2003). $Nrarp^{-/-}$ mice are viable with normal life span. $Nrarp^{-/-}$ females show reduced fertility. In retinal angiogenesis, *Nrarp* mutants display defects in the radial expansion of the vascular plexus from the optic nerve head to the periphery. Quantification reveals a significant delay in radial expansion in both $Nrarp^{-/-}$ and $Nrarp^{+/-}$ retinas (Figures 2A–2D; **, $p < 0.01$; *, $p < 0.05$). The delay in radial expansion is still observed at P7 (not shown), but partially resolves by P10, indicating that loss of Nrarp reduces the speed of vascular growth rather

than causing an inability to progress. We also observed a significant reduction in vessel density in *Nrarp*$^{+/-}$ and *Nrarp*$^{-/-}$ retinas (Figures 2E–2H), which was most severe close to arteries and the vascular front. At higher magnification, vessel profiles of *Nrarp*$^{-/-}$ retinas are conspicuously narrow at branch points and appear unstable and poorly lumenized. Vascular sprouts of *Nrarp*$^{+/-}$ and *Nrarp*$^{-/-}$ mice (arrowheads, Figures 2J and 2K) were generally more slender compared to those of *Nrarp*$^{+/+}$ mice (Figure 2I). The number of filopodia per 100 μm of leading endothelial membrane was not affected (Figure 2L), suggesting that sprouting activity is not affected by loss of *Nrarp*. Most of the defects in retinal angiogenesis resolve over time, and by P14 all three layers of vessels are present, although some mild patterning defects remain (Figure S3).

Loss of *nrarp-a* and *nrarp-b* in Zebrafish Leads to Defects in Intersegmental Vessel Patterning

To study the function of *nrarp* in zebrafish intersegmental vessel (ISV) development, we injected morpholinos that block the translation of *nrarp-a* and *–b* transcripts (Ishitani et al., 2005) into *Tg(fli1:EGFP)*^{y1} embryos in which the vascular endothelium is visualized by eGFP expression (Lawson and Weinstein, 2002). At ~56 hpf, control morpholino-injected embryos develop ISVs that extend dorsally between somite boundaries on both sides of the notochord and form the dorsal longitudinal anastomotic vessel (DLAV) (Figure 3A). In *nrarp-a* and *nrarp-b* morphants, ISVs reach the dorsal roof of the neural tube (Figures 3B and 3C) but show irregular and often thin diameter as well as poor connection to the DA and the DLAV (Figures 3B–3H). Disconnections occur most frequently at the boundary of ISV and the DA in *nrarp-a* morphants and between the ISV and DLAV in *nrarp-b* morphants (Figure 3L). Combined knockdown of *nrarp-a* and *nrarp-b* leads to similar vessel disconnections as well as the formation of misguided vessels (yellow arrowhead, Figure 3D).

Labeling of somite boundaries with an antibody against collagen XII (Bader et al., 2008) illustrated that *nrarp-a* and *-b* and double *nrarp-a* and *-b* morphants display discontinuous ISVs in the presence of intact segment boundaries (arrows, Figures 3E–3H), suggesting that ISV malformations are caused by loss of endothelial *nrarp* functions and not secondary consequences of segmentation defects.

Loss of *nrarp-a* and *nrarp-b* in Zebrafish and *Nrarp* in Mouse Results in Ectopic Vessel Regression

Time-lapse confocal laser scanning microscopy of the morphants from 48 hpf onward revealed that disconnections result from EC retraction and consequent regression. In control morphants, the ISVs remained connected with the DA and the DLAV (Figure 3I; Movie S1). *nrarp-a* knockdown resulted in gradual regression of ISV from the existing DLAV (Figure 3J; Movie S2). Also, *nrarp-b* knockdown frequently led to regression of the ISV from the DA and also from the DLAV (Figure 3K; Movie S3). The observed dynamic regression may explain the missing ISVs occasionally observed in *nrarp-a* and *nrarp-b* morphants (Figure 3G).

In fixed tissue, empty basement membrane sleeves labeled for collagen IV but lacking endothelial markers faithfully highlight vessel regression (Baffert et al., 2006). At the sprouting front of P5 *Nrarp*$^{+/+}$ retinas, collagen IV colocalizes with endothelial Isolectin-B4 (Figure 4A) or Endomucin staining (data not shown), suggesting that newly formed vessels in the vicinity of high VEGF production rarely regress. In the more central plexus, most vessels show both collagen IV and Isolectin-B4 staining; however, closer to arteries, collagen IV profiles lacking Isolectin-B4 indicate regression profiles (Figure S4). In P5 *Nrarp*$^{+/-}$ and *Nrarp*$^{-/-}$ retinas, we observed more vessel regression profiles in the remodeling plexus (arrowheads in Figure 4D′ and 4E; $p < 0.0005$), and also at the sprouting front (arrowheads in Figure 4B), suggesting that *Nrarp* deficiency induces pruning even in regions of high VEGF stimulation. The observed vessel regression in the sprouting region could explain the delayed retinal vascularization and the reduced vascular density in *Nrarp*-deficient retinas.

EC adherens and tight junctions are essential for stabilization of vessel morphology and structure (Blum et al., 2008; Corada et al., 1999). Claudin 5, an endothelial tight junction component, localizes to junctions along the length of patent vessels in a continuous manner (Morita et al., 1999). During vessel regression, continuous junctions are disrupted and Claudin 5 redistributes to cytoplasmic vesicular structures (Figure S4).

In *Nrarp*$^{+/+}$ mice, a continuous network of junctions decorates the capillary plexus (Figure 4C), whereas in *Nrarp*$^{-/-}$ mice, the junctional network is fragmented with frequently isolated Claudin 5 strands and punctate structures (Figures 4D and 4D″).

Endothelial junctions are similarly disorganized between ISVs and DA in zebrafish *nrarp-a* and *nrarp-b* morphants. At 48 hpf in uninjected embryos, two ECs form two parallel strands that connect in a ring-shaped junction with ECs of the DA (Figures 4F, 4F′, and 4F″), as revealed by zona occludens 1 (ZO1) staining (Blum et al., 2008). In *nrarp-a* and *b* morphants, we frequently observe single junctional strands without ring-shaped connection to the DA (Figures 4G, 4G′, and 4G″ and data not shown).

Decreased EC Proliferation in Zebrafish *nrarp-a* and *nrarp-b* Morphants and *Nrarp*$^{-/-}$ Mice

In the zebrafish, ECs of the ISVs undergo controlled proliferation. In the absence of Notch signaling, more ECs proliferate and adopt the explorative migrating tip cell behavior, leading to excessive numbers of ECs in the ISVs (Leslie et al., 2007; Siekmann and Lawson, 2007). In the mouse, loss of Notch signaling also leads to excessive formation of endothelial tip cells (Hellstrom et al., 2007b; Suchting et al., 2007) and increased EC proliferation (Hellstrom et al., 2007b; Lobov et al., 2007; Siekmann and Lawson, 2007). We therefore investigated whether *Nrarp* has a role in regulating EC proliferation.

Tg(fli1:EGFP)^{y1} zebrafish embryos were exposed to BrdU between 19 and 48 hpf. ECs that divided during this period are detected by BrdU staining and GFP expression. In control morphants, all ECs within the ISV showed BrdU incorporation (99%; Figures 5A and 5D), whereas the ratio of BrdU-positive ECs was only ~80% in *nrarp-a* and *nrarp-b* morphants (Figures 5B–5D). In some ISVs, none of the ECs were BrdU labeled, indicating that these ISVs formed solely by migrating ECs in the absence of proliferation.

The significant decrease in EC proliferation offers an explanation for the decreased number of ECs that constitute the ISVs in *nrarp-a* and *nrarp-b* morphants. In control embryos, ISVs comprise of 1–6 ECs, with the largest fraction (35.5%) lined by 4 EC nuclei (Figure 5E). In *nrarp-a* and *nrarp-b* morphants, most ISVs contain only 2 EC nuclei (*nrarp-a* MO, 43%; *nrarp-b* MO, 41%; Figure 5E). Occasionally, the cellular compartment containing the nucleus shifted to contribute to the DLAV, while the remaining ISV consisted of a nucleus-free cytoplasmic trail (data not shown).

Endothelial proliferation is also reduced in *Nrarp*$^{-/-}$ retinas at P5 (Figures 5F and 5I; p = 0.0328), suggesting that *Nrarp* controls EC proliferation during sprouting angiogenesis in mouse and zebrafish.

Loss of Nrarp Leads to Increased Notch Signaling and Reduced Wnt Signaling in Endothelial Cells

Nrarp has been reported to act as a negative regulator of Notch signaling by destabilizing the Notch intracellular domain (Ishitani et al., 2005; Lamar et al., 2001). Consistent with this concept, *Nrarp*$^{-/-}$ retinas reveal mildly elevated levels of the cleaved Notch1 intracellular domain (NICD1) (Figure 6A) and increased mRNA levels of the Notch target genes *Hey2* and *Lunatic fringe* (*Lnfg*) (Figure 6B; *Hey2*, p = 0.0426; *Lnfg*, p = 0.0025). A slight but significant increase in *Lngf* mRNA in *Nrarp*$^{+/-}$ retinas (Figure 6B, p = 0.015) suggests a dose-dependent negative regulation of Notch signaling through Nrarp. To directly test whether Nrarp influences Notch signaling in ECs, we silenced *NRARP* in HUVECs (Figure S5) by specific small interfering RNA (siRNA) and monitored Notch-signaling activity using the TP-1 luciferase Notch-reporter (Minoguchi et al., 1997). HUVECs transfected with scrambled control siRNA show a robust (8-fold) increase in TP-1 reporter activity when plated on immobilized Dll4 (Figure 6C, lane 3). *NRARP* knockdown significantly augments this induction (Figure 6C, lane 4), demonstrating that Nrarp limits Notch signaling in ECs.

Ectopic activation of Notch signaling in the postnatal retina reduces vascular density through inhibition of endothelial tip cell formation and filopodia extension (Hellstrom et al., 2007b). Although *Nrarp*$^{-/-}$ retinas display normal filopodia numbers (Figure 2L), it is possible that the increased Notch signalling directly limits vascular density. Forty-eight hour pharmacological reduction of Notch signaling by DAPT treatment restored vascular density to near normal levels in *Nrarp*$^{-/-}$ retinas (Figures 6D–6F and Figure S6C) while causing the reported hyperdense, hypersprouting vasculature in *Nrarp*$^{+/+}$ and *Nrarp*$^{+/-}$ retinas (Hellstrom et al., 2007b; Suchting et al., 2007). The abnormal stalk cell morphology including reduced sprout diameter and poor vessel connections persisted in *Nrarp*$^{-/-}$ retinas after DAPT treatment (Figure 6F), indicating that the excessive regression is not caused by increased Notch activity. By studying sprout diameter and collagen IV distribution 48 hr after treatment with the Jagged1 (huJag1) peptide, we found no evidence for increased vessel regression (Figure S7). Together, these results imply that negative regulation of Notch signaling is not the only function of Nrarp in ECs and that the observed vascular regression may be linked to an additional role of Nrarp in angiogenesis.

Ishitani et al. reported that zebrafish nrarp-a binds to and stabilizes lymphoid enhancer factor 1 (Lef1) by preventing its degradation, leading to a positive modulation of Wnt signaling

during zebrafish neural crest differentiation (Ishitani et al., 2005). Western blot analysis shows reduced Lef1 protein in *Nrarp*$^{+/-}$ and *Nrarp*$^{-/-}$ retinas (Figure 6G), suggesting that Nrarp also regulates Lef1 in the mouse. Myc-tagged Nrarp coimmunoprecipitates with Lef1, confirming the interaction of Nrarp and Lef1 in ECs (Figure 6H). Isolated primary mouse ECs from *Nrarp*$^{-/-}$ mice express significantly less *Cyclin D1* (Figure 6I), which, in addition to being an important cell cycle regulator, is a known transcriptional target of Ctnnb1/Lef1-dependent Wnt signaling (Shtutman et al., 1999). Conversely, the Notch-target *Hey2* is highly overexpressed in *Nrarp*$^{-/-}$ ECs, together indicating that Nrarp also differentially modulates Notch and Wnt signaling in mouse ECs.

To directly test this idea, we transfected HUVECs with the super8xTOPFlash Wnt signaling luciferase reporter (Veeman et al., 2003) and measured the activity of Wnt3a and/or Dll4 stimulated cells treated with *NRARP* or scrambled siRNA. Wnt3a stimulation induces significant Wnt-reporter activity, which is abolished by *NRARP* knockdown (Figure 6J). Dll4 treatment alone does not activate the reporter; however, costimulation with Wnt3a and Dll4 leads to an even more pronounced activation of Wnt signaling, which is abolished by *NRARP* knockdown.

Based on these data, Notch-induced Nrarp expression could potentially regulate vessel stability by promoting Wnt signaling in endothelial stalk cells. Studying retinas of the Wnt signaling reporter mouse, BAT-gal (Maretto et al., 2003), we observed strong Wnt signaling as evidenced by β-galactosidase expres sion specifically in ECs situated behind the sprouting front and in the vascular plexus (Figures 6K and 6L). The strongest reporter activity regularly localized to ECs situated at branch points, strikingly similar to the expression pattern of *Nrarp*.

Loss of *Lef1* and Endothelial-Specific Deletion of *Ctnnb1* Cause Excessive Retinal Vessel Regression

Analysis of *Lef1*$^{-/-}$ mouse retinas reveals delayed peripheral vascularization and reduced vessel density similar to the phenotype observed in *Nrarp*$^{-/-}$ mice (Figures 7A–7D and 7I). Discontinuous and fragmented vessels at the sprouting vascular front indicate extensive vessel regression, which is confirmed by collagen IV labeling (Figures 7E–7H and 7J). Junctional Claudin 5 labeling illustrates discontinuities as observed in *Nrarp*$^{-/-}$ retinas, together suggesting that the loss of Nrarp or Lef1 causes vessel instability.

Lef1 forms a complex with nuclear Ctnnb1 to control transcription of target genes of the canonical Wnt signaling pathway (Hsu et al., 1998). Recent studies suggested additional functions for Lef1 independent of components of the Wnt signaling pathway (Eastman and Grosschedl, 1999; Ross and Kadesch, 2001). To directly test the potential involvement of Ctnnb1, we deleted *Ctnnb1* during postnatal retinal angiogenesis from ECs using *Ctnnb1*$^{lox/lox}$ mice (Brault et al., 2001) crossed to the tamoxifen-inducible *Pdgfb-iCreER IRES-EGFP* line (Claxton et al., 2008). EGFP detection confirmed endothelial-specific expression of Cre in the retina, and crosses with the Cre-reporter line *Rosa26R-EYFP* (Srinivas et al., 2001) illustrated efficient Cre-mediated recombination 24–72 hr after a single injection of tamoxifen (data not shown). Deletion of *Ctnnb1* for 48 or 72 hr resulted in a significant reduction in vascular density (Figures 7M–7Q). While sprouting occurs

normally, empty basement membrane sleeves indicate excessive vessel regression (Figures 7N, 7P, and 7R). We observed similar defects in retinas of mice deficient in the low-density lipoprotein receptor-related protein 5 (Lrp5) (Figure S8), which functions as essential coreceptor in canonical Wnt signaling (He et al., 2004), together suggesting that endothelial Wnt signaling controls vascular stability.

Ctnnb1 also plays a role in stabilizing adhesion junctions in epithelial and ECs through its association with cadherins. However, loss of endothelial *Ctnnb1* does not cause junctional disassembly due to redundant activity of γ-catenin and increased incorporation of desmoplakin (Cattelino et al., 2003). We observed a similar level and distribution of VE-cadherin and ZO-1 in Cre+ and – retinas (Figures 7S and 7T; Figure S9), despite a complete absence of junctional Ctnnb1.

DISCUSSION

Our study of Nrarp function in mouse and zebrafish provides an insight into the mechanisms regulating vessel stability during sprouting angiogenesis: Dll4/Notch signaling induces expression of Nrarp in the stalk cells, where it differentially modulates Notch- and Wnt signaling activity to balance stalk cell proliferation and maintain vessel stability during network formation.

The increase in NICD levels and Notch target gene expression in *Nrarp*$^{-/-}$ retinas and isolated ECs is in line with earlier findings illustrating that Nrarp negatively regulates Notch signaling by promoting NICD degradation (Ishitani et al., 2005; Lamar et al., 2001; Yun and Bevan, 2003). Dll4-Notch signaling induces Nrarp expression, and siRNA-mediated knockdown of *NRARP* in HUVECs augments activity of the TP-1 luciferase Notch-signaling reporter. Thus, increased Notch signaling in endothelial stalk cells correlates with vessel regression, whereas reduced Notch signaling in the stalk leads to formation of a new tip cell (Hellstrom et al., 2007b; Leslie et al., 2007; Lobov et al., 2007; Suchting et al., 2007). Balancing Notch activity could therefore regulate the fate of endothelial stalk cells: deciding whether to add a new branch or to take away an existing branch.

VEGF-A and Notch signaling engage in a feedback loop controlling reiterative induction, elongation, branching, and anastomosis of vascular sprouts (Hellstrom et al., 2007a; Leslie et al., 2007). Vascular pruning occurs subsequently in regions of lower VEGF-A, and oxygenation-dependent reduction of VEGF-A levels is a contributing factor (Claxton and Fruttiger, 2003, 2005). Blocking VEGF-A signaling in adult mice appears sufficient to induce rapid vessel pruning (Baffert et al., 2006; Inai et al., 2004). In *Nrarp*$^{-/-}$ retinas, however, excessive vessel regression occurs in regions of high VEGF-A expression concomitant with sprouting, suggesting that the loss of Nrarp disables a molecular pathway that normally stabilizes vessels under VEGF-A stimulation. Several groups reported regulation of VEGF receptor expression through Notch signaling. *Vegfr2* expression is induced by VEGF-A and downregulated in ECs through Notch signaling (Harrington et al., 2007). Thus, vascular regression in *Nrarp*$^{-/-}$ retinas could be mediated by Notch-dependent repression of *Vegfr2*. However, qPCR analysis showed normal *VEGF-A* and slightly increased *Vegfr2* expression in *Nrarp*$^{-/-}$ retinas (Figure S13). VEGFR1 (Flt1), which

functions as a high-affinity decoy receptor for VEGF-A, is upregulated by Notch signaling (Harrington et al., 2007). *Nrarp*$^{-/-}$ retinas express higher levels of *Flt1* mRNA (Figure S10), suggesting that enhanced Flt1-mediated sequestration of VEGF-A could contribute to the reduced EC proliferation and vessel density.

Vessel stability further requires pericyte investment, the loss of which leads to selective vessel regression (Hammes et al., 2002). *Nrarp* mRNA was not detected in retinal pericytes, and vessel regression in *Nrarp*$^{-/-}$ retinas occurs despite apparently normal pericyte recruitment (Figure S11), suggesting that the vascular phenotype in *Nrarp*$^{-/-}$ retinas reflects an EC-autonomous role of Nrarp in vessel stabilization.

Our observations illustrate that the cellular mechanism of vessel regression involves reduced endothelial proliferation and excessive junctional remodeling. Activation of Notch signaling in ECs induces cell cycle arrest through retinoblastoma protein dephosphorylation and downregulation of p21CIP (Noseda et al., 2004). Wnt signaling promotes EC proliferation (Masckauchan et al., 2005, 2006) and the Lef1/Ctnnb1 complex induces cell cycle progression through transcriptional activation of *Cyclin D1* (Shtutman et al., 1999). Isolated ECs from *Nrarp*$^{-/-}$ mice show increased expression of the Notch-target *Hey2* and significantly reduced expression of *Cyclin D1* (Figure 6). Thus, Nrarp could drive endothelial stalk cell proliferation by limiting Notch-dependent cell cycle arrest and increasing Lef1/Wnt signaling-dependent Cyclin D1 levels. The function of Nrarp could therefore explain why endothelial stalk cells readily proliferate although they receive highest levels of Notch activation through Dll4 signaling from the leading tip cells.

The identity of the relevant Wnt ligands and Fzd receptors involved upstream of Lef1/Ctnnb1 in the retinal endothelial Wnt signaling modulated by Nrarp remain to be identified. The involvement of Lef1, Lrp5, and Ctnnb1 in vivo and the regulation of Wnt3a-dependent TOPFlash reporter activity by Nrarp ex vivo point toward canonical Wnt signaling as a regulator of stalk cell and branch point stability. A C-terminal truncating mutation in the Lrp5 gene, abrogating its activity in Wnt signaling, causes retinal vascular defects including collapsed lumen and attenuated vascularization (Xia et al., 2008). Loss of Norrin-dependent activation of Fzd4 also causes defects in retinal vascularization (Xu et al., 2004). Whereas Norrin, Fzd4, or Lrp5 deficiency leads to severe and persistent attenuation of retinal vascularization, most of the defects caused by the loss of Nrarp resolve after the first postnatal week. One conceivable explanation is that Nrarp is a modulator of Wnt signaling, the loss of which leads to reduced signaling as opposed to complete loss caused by deletion of upstream components. Nevertheless, the loss of one allele of *Nrarp* already leads to vessel regression, and reducing *NRARP* expression by siRNA in HUVECs abrogates Wnt3a induced TOPFlash reporter activation.

Endothelial Ctnnb1 is required for vessel stability likely through interaction with Lef1 (Figure 6). Constitutive activation of one or two copies of the *Ctnnb1*$^{lox(Ex3)}$ allele (Harada et al., 1999) in *Nrarp*$^{-/-}$ mice using the tamoxifen-inducible *Pdgfb-iCreER* line did not consistently reduce the regression (Figure S12), suggesting that Ctnnb1 activation is required for vessel stability but is not sufficient in the absence of Nrarp.

In conclusion, we propose, based on our study of Nrarp function in mouse and zebrafish, that Wnt and Notch pathways integrate in endothelial stalk cells of newly formed vessels to control vascular sprouting and regression in angiogenesis.

EXPERIMENTAL PROCEDURES

Animals

To generate *Nrarp* null mice, the genomic coding region of the gene was replaced by a LacZ-Neomycin cassette (Figure S1). *Nrarp*, *Ctnnb1*^{lox} (described in Brault et al., 2001), *Pdgfb-iCreER* (Claxton et al., 2008), and BAT-gal (Maretto et al., 2003) transgenic mice were backcrossed to C57Bl6/J. *Lef1* mice were bred in a C57Bl6×129Sv hybrid background. 4OH-tamoxifen was injected intraperitoneally into early postnatal pups at 80 μg/g to activate Cre recombination. *Tg(fli1:EGFP)*^{y1} zebrafish were raised and maintained under standard conditions.

Morpholino Knockdown of *nrarp-a* and *nrarp-b* in Zebrafish

Antisense morpholino oligonucleotides (Gene Tools) were diluted in Danieau buffer containing 0.2% phenol red. Oligonucleotide (10ng) was injected into the yolk of 2–4 cell stage *Tg(fli1:EGFP)*^{y1} embryos. Morpholino sequences: *nrarp-a*, 5′-GATGCTTCACACTGGGAGAAACTCG-3′ and *nrarp-b*, 5′-ATGATTTCAGCAGGTTGACCAAAACG-3′ (Ishitani et al., 2005). The control morpho lino used is the standard control provided by Gene Tools.

Whole-Mount In Situ Hybridization

Retina in situ hybridization (ISH) was previously described (Fruttiger, 2002). Primers to generate mouse *Nrarp* probe: forward 5′-ctagctctgcggcaacatga-3′ and reverse 5′-gagcccggtaatggttgttt-3′. Retinas were counterstained with Isolectin-B4 after ISH. Zebrafish ISH was performed as described (Ariza-McNaughton and Krumlauf, 2002). *nrarp-a* probe was provided by Ertugrul Ozbudak.

Immunofluorescence

Eyes were fixed in 4% paraformaldehye (PFA). For anti-claudin 5 staining, mice were exsanguinated by transcardiac perfusion of PBS before dissecting and fixing retinas in methanol. Antibodies were diluted in PBSa containing 0.5% BSA and 0.25% Tween 20 except for Isolectin-B4 and endomucin, which were diluted in PBlec (PBS [pH6.8], 1% Triton X-100, 0.1 mM $CaCl_2$, 0.1 mM $MgCl_2$, 0.1 mM $MnCl_2$). Primary antibodies used: biotinylated-Isolectin-B4 (Sigma), collagen IV (AbD Serotec), BrdU (Molecular Probes), β-galactosidase (Biogenesis), endomucin (Dietmar Vestweber), GFP (Molecular Probes), claudin 5 and human ZO1 (Zymed), Ctnnb1 (BD Transduction), and zebrafish collagen XII. Alexa-488, −568 or −633 conjugated secondary antibodies were used (Molecular Probes).

Proliferation Assay

Tg(fli1:EGFP)^{y1} zebrafish embryos were exposed to 0.5% bromodeoxyuridine (BrdU, Sigma) in E3 buffer (5 mM NaCl, 0.17 mM KCl, 0.33 mM $CaCl_2$, 0.33 mM $MgSO_4$) from

19 hpf to 48 hpf and fixed in 4% PFA. Embryos were dehydrated and permeabilized in 100% MeOH at −20°C, incubated in 20% DMSO in MeOH, rehydrated in PBT, incubated in 2 N HCl, and then stained for BrdU. In mouse, BrdU was administered at 10 mg/kg intraperitoneally at P5 for 3 hr. For BrdU labeling, retinas were digested with Proteinase K (10 μg/ml), fixed in 4% PFA, treated with DNase I (0.1 U/μl) for 2 hr at 37°C, and incubated with anti-BrdU antibody. The number of BrdU-positive ECs in 10,000 μm^3 volume of vessels (measured using Volocity, Improvision, UK) at the vascular front was determined.

Animal Procedures

DAPT (Merck) was injected subcutaneously at 100 mg/kg once for 6 hr treatment or once a day for 2 days for 48 hr treatment. Dll4-Fc or hFc (4 μg) was injected once per eye for 24 hr (see Gerhardt et al., 2003, for procedure).

Cell Culture and Transfections

Pooled human umbilical vein ECs (HUVEC) were purchased from Lonza and cultured in endothelial basal medium (EBM; Lonza) supplemented with hydrocortisone (1 μg/ml), bovine brain extract (12 μg/ml), gentamicin (50 μg/ml), amphotericin B (50 ng/ml), EGF (10 ng/ml), and 10% fetal calf serum (FCS; GIBCO) until the third passage. Lung ECs (MLEC) from adult *Nrarp*$^{+/+}$ and *Nrarp*$^{-/-}$ mice were isolated by Dispase II (2.4 U/ml; GIBCO) digestion for 1 hr, incubation with rat α-PECAM-1 antibody, separation with goat-α-rat magnetic beads (Miltenyi Biotec), and cultured on rDll4 (1 μg/ml, R&D Systems) coated dishes in EC growth medium MV (PromoCell) supplemented with ECGs/H (0.4%), EGF (0.1 ng/ml), Hydrocortison (1 μg/ml), bFGF (1ng/ml), amphotericin B (50 ng/ml), and FCS (10%).

Plasmid transfections in HUVEC were performed by using the Targefect F2 and Virofect reagents (Targeting Systems) according to the manufacturers' protocols and as previously described (Potente et al., 2005). mNrarp-Myc (MT) construct was kindly provided by Motoyuki Itoh, Nagoya, Japan. Recombinant human Dll4 (500 ng/ml) and Wnt3a (100 ng/ml) were from R&D Systems.

RNA Interference

A validated pool of siRNA molecules directed against human *NRARP* (On-Target plus SMART pool) was purchased from Dharmacon. HUVECs were transfected with siRNAs (50–100 nM) against *NRARP* or a scrambled control siRNA using the GeneTrans II reagent (MoBiTec) as previously described (Potente et al., 2005, 2007). For combined gene knockdown and reporter assay in HUVECs (see below), highest efficacy was achieved by sequential siRNA and reporter plasmid transfection using distinct reagents and protocols (GeneTrans II for siRNA and Targefect F2/Virofect for reporter plasmids).

Reporter Assays

Reporter assays in HUVECs were performed with the Dual-Luciferase Reporter Assay System (Promega) and a LUMAT LB 9507 luminometer (BERTHOLD Technologies) according to the manufacturers' protocols. Briefly, 24 hr after siRNA transfection, HUVECs were transfected with either TOPFLASH or TP1 luciferase reporters and the constitutive

Renilla luciferase reporter pGL4.74*hRluc*/TK (Promega) to control for transfection efficiency. Luciferase activities were determined 24 hr after transfection. TP1 or TOPFLASH reporter activity was adjusted for the internal Renilla luciferase control and is expressed relative to control.

Relative Quantitative PCR

RNA from retinas and HUVECs was reverse transcribed using SuperScript III (Invitrogen). TaqMan Gene Expression Cells-to-Ct Kit (Applied Biosystems) was used to prepare cDNA from MLECs for qPCR. *Nrarp/NRARP*, *Hey1*, *Hey2*, *Lunatic Fringe*, *CyclinD1*, *VEGFA*, *Flt1*, and *Kdr* TaqMan Gene Expression Assays were obtained from Applied Biosystems, and qPCR was carried out using Applied Biosystems 7900HT sequence detection system or StepOnePlus real-time PCR system. Gene expression was normalized to the endogenous control, β-*actin*.

Immunoprecipitation, SDS-PAGE, and Western Blotting

Total cell lysates from HUVECs were prepared in IPLS buffer (50 mM Tris-HCl [pH 7.5], 120 mM NaCl, 0.5 mM EDTA, 0.5% Nonidet P-40, protease inhibitor mixture), and immunoprecipitations were carried out as described in Martin et al. (2008). Retinas were lysed in RIPA buffer (50 mM Tris-HCl [pH 7.5], 150 mM NaCl, 1 mM EDTA, 1% Nonidet P-40, 0.25% Na-deoxycholate, and protease inhibitor mixture). SDS-PAGE and western blot analysis were performed according to standard procedures. Antibodies used: cleaved Notch1 (Val1744, Cell Signaling), mouse α-LEF1 (Chemicon), rabbit α-LEF1 (Cell Signaling), α-Myc (Santa Cruz Biotechnology), α-actin (Sigma), Tubulin (Neomarkers), and sheep α-mouse or α-rabbit HRP-conjugated antibodies (GE Healthcare). Horseradish peroxidase activity was revealed by a chemoluminescence reaction (ECL, GE Healthcare). Densitometric analysis of blots was performed by using ImageJ (Version 1.38x).

Microscopy

Confocal laser scanning microscopy was performed using Zeiss LSM 510 Meta microscope. For live imaging of *Tg(fli1:EGFP)*^{y1} zebrafish, the embryos were anaesthetized in aquarium water containing 320 μg/ml Tricaine (Sigma), mounted on a glass-bottom dish (MatTek) in 0.2% agarose, and kept at 28°C. Images were captured with a Zeiss LSM 510 confocal microscope using a 40× water immersion objective lens.

Quantification of Vessel Migration, Density, and Regression in Mouse Retina

For vessel migration, the distance of vessel growth from the optic nerve to the periphery was measured. *n* indicates number of animals. For vessel density, the number of vessel branch points in 100 μm^2 field was counted. *n* indicates number of images. For vessel regression, the skeletal length of Isolectin-B4-positive and collagen IV-positive vessels was measured and the ratio calculated. *n* indicates number of images.

Statistical Analysis

Statistical analysis was performed with Prism 5 software (GraphPad) using two-tailed, unpaired t test.

Supplementary Material

Refer to Web version on PubMed Central for supplementary material.

ACKNOWLEDGMENTS

We thank Sue Watling, Craig Thrussell, and Claire Darnbrough for help with mouse care and experiments; Phil Taylor for fish care; Florence Ruggiero and Hanah Bader, Lyon, for providing the collagen XII antibody and staining protocol; Motoyuki Itoh, Nagoya, for providing the Myc-tagged Nrarp plasmid; and Michael Way for critical reading of the manuscript. We acknowledge the Light Microscopy Service, London Research Institute for use of imaging equipment. This work was funded by Cancer Research UK (L.K.P., J.D.L., J.B., H.G.), the EMBO Young Investigator Program (H.G.), and the Lister Institute of Preventive Medicine (H.G). D.N. is supported by the Swedish Research Council and Associazione Italiana for Cancer Research. M.P. is supported by the DFG (PO1306/1-1 and Exc 147/1). G.T. and I.L. are employees of Regeneron Pharmaceuticals.

REFERENCES

Ariza-McNaughton L, and Krumlauf R (2002). Non-radioactive in situ hybridization: simplified procedures for use in whole-mounts of mouse and chick embryos. Int. Rev. Neurobiol 47, 239–250. [PubMed: 12198801]

Bader HL, Keene DR, Charvet B, Veit G, Driever W, Koch M, and Ruggiero F (2008). Zebrafish collagen XII is present in embryonic connective tissue sheaths (fascia) and basement membranes. Matrix Biol., in press.

Baffert F, Le T, Sennino B, Thurston G, Kuo CJ, Hu-Lowe D, and McDonald DM (2006). Cellular changes in normal blood capillaries undergoing regression after inhibition of VEGF signaling. Am. J. Physiol. Heart Circ. Physiol 290, H547–H559. [PubMed: 16172161]

Blum Y, Belting HG, Ellertsdottir E, Herwig L, Luders F, and Affolter M (2008). Complex cell rearrangements during intersegmental vessel sprouting and vessel fusion in the zebrafish embryo. Dev. Biol 316, 312–322. [PubMed: 18342303]

Brault V, Moore R, Kutsch S, Ishibashi M, Rowitch DH, McMahon AP, Sommer L, Boussadia O, and Kemler R (2001). Inactivation of the beta-catenin gene by Wnt1-Cre-mediated deletion results in dramatic brain malformation and failure of craniofacial development. Development 128, 1253–1264. [PubMed: 11262227]

Cattelino A, Liebner S, Gallini R, Zanetti A, Balconi G, Corsi A, Bianco P, Wolburg H, Moore R, Oreda B, et al. (2003). The conditional inactivation of the beta-catenin gene in endothelial cells causes a defective vascular pattern and increased vascular fragility. J. Cell Biol 162, 1111–1122. [PubMed: 12975353]

Claxton S, and Fruttiger M (2003). Role of arteries in oxygen induced vaso-obliteration. Exp. Eye Res 77, 305–311. [PubMed: 12907163]

Claxton S, and Fruttiger M (2005). Oxygen modifies artery differentiation and network morphogenesis in the retinal vasculature. Dev. Dyn 233, 822–828. [PubMed: 15895398]

Claxton S, Kostourou V, Jadeja S, Chambon P, Hodivala-Dilke K, and Fruttiger M (2008). Efficient, inducible Cre-recombinase activation in vascular endothelium. Genesis 46, 74–80. [PubMed: 18257043]

Corada M, Mariotti M, Thurston G, Smith K, Kunkel R, Brockhaus M, Lampugnani MG, Martin-Padura I, Stoppacciaro A, Ruco L, et al. (1999). Vascular endothelial-cadherin is an important determinant of microvascular integrity in vivo. Proc. Natl. Acad. Sci. USA 96, 9815–9820. [PubMed: 10449777]

Eastman Q, and Grosschedl R (1999). Regulation of LEF-1/TCF transcription factors by Wnt and other signals. Curr. Opin. Cell Biol 11, 233–240. [PubMed: 10209158]

Fruttiger M (2002). Development of the mouse retinal vasculature: angiogenesis versus vasculogenesis. Invest. Ophthalmol. Vis. Sci 43, 522–527. [PubMed: 11818400]

Gerhardt H, Golding M, Fruttiger M, Ruhrberg C, Lundkvist A, Abramsson A, Jeltsch M, Mitchell C, Alitalo K, Shima D, et al. (2003). VEGF guides angiogenic sprouting utilizing endothelial tip cell filopodia. J. Cell Biol 161, 1163–1177. [PubMed: 12810700]

Gridley T (2007). Notch signaling in vascular development and physiology. Development 134, 2709–2718. [PubMed: 17611219]

Hammes HP, Lin J, Renner O, Shani M, Lundqvist A, Betsholtz C, Brownlee M, and Deutsch U (2002). Pericytes and the pathogenesis of diabetic retinopathy. Diabetes 51, 3107–3112. [PubMed: 12351455]

Harada N, Tamai Y, Ishikawa T, Sauer B, Takaku K, Oshima M, and Taketo MM (1999). Intestinal polyposis in mice with a dominant stable mutation of the beta-catenin gene. EMBO J. 18, 5931–5942. [PubMed: 10545105]

Harrington LS, Sainson RC, Williams CK, Taylor JM, Shi W, Li JL, and Harris AL (2007). Regulation of multiple angiogenic pathways by Dll4 and Notch in human umbilical vein endothelial cells. Microvasc. Res 75, 144–154. [PubMed: 17692341]

He X, Semenov M, Tamai K, and Zeng X (2004). LDL receptor-related proteins 5 and 6 in Wnt/beta-catenin signaling: arrows point the way. Development 131, 1663–1677. [PubMed: 15084453]

Hellstrom M, Phng LK, and Gerhardt H (2007a). VEGF and Notch signaling: the Yin and Yang of angiogenic sprouting. Cell Adh. Migr 1, 133–136. [PubMed: 19262131]

Hellstrom M, Phng LK, Hofmann JJ, Wallgard E, Coultas L, Lindblom P, Alva J, Nilsson AK, Karlsson L, Gaiano N, et al. (2007b). Dll4 signalling through Notch1 regulates formation of tip cells during angiogenesis. Nature 445, 776–780. [PubMed: 17259973]

Hsu SC, Galceran J, and Grosschedl R (1998). Modulation of transcriptional regulation by LEF-1 in response to Wnt-1 signaling and association with beta-catenin. Mol. Cell. Biol 18, 4807–4818. [PubMed: 9671490]

Inai T, Mancuso M, Hashizume H, Baffert F, Haskell A, Baluk P, Hu-Lowe DD, Shalinsky DR, Thurston G, Yancopoulos GD, et al. (2004). Inhibition of vascular endothelial growth factor (VEGF) signaling in cancer causes loss of endothelial fenestrations, regression of tumor vessels, and appearance of basement membrane ghosts. Am. J. Pathol 165, 35–52. [PubMed: 15215160]

Ishitani T, Matsumoto K, Chitnis AB, and Itoh M (2005). Nrarp functions to modulate neural-crest-cell differentiation by regulating LEF1 protein stability. Nat. Cell Biol 7, 1106–1112. [PubMed: 16228014]

Krebs LT, Deftos ML, Bevan MJ, and Gridley T (2001). The Nrarp gene encodes an ankyrin-repeat protein that is transcriptionally regulated by the notch signaling pathway. Dev. Biol 238, 110–119. [PubMed: 11783997]

Lamar E, Deblandre G, Wettstein D, Gawantka V, Pollet N, Niehrs C, and Kintner C (2001). Nrarp is a novel intracellular component of the Notch signaling pathway. Genes Dev. 15, 1885–1899. [PubMed: 11485984]

Lawson ND, and Weinstein BM (2002). In vivo imaging of embryonic vascular development using transgenic zebrafish. Dev. Biol 248, 307–318. [PubMed: 12167406]

Leslie JD, Ariza-McNaughton L, Bermange AL, McAdow R, Johnson SL, and Lewis J (2007). Endothelial signalling by the Notch ligand Delta-like 4 restricts angiogenesis. Development 134, 839–844. [PubMed: 17251261]

Liu ZJ, Shirakawa T, Li Y, Soma A, Oka M, Dotto GP, Fairman RM, Velazquez OC, and Herlyn M (2003). Regulation of Notch1 and Dll4 by vascular endothelial growth factor in arterial endothelial cells: implications for modulating arteriogenesis and angiogenesis. Mol. Cell. Biol 23, 14–25. [PubMed: 12482957]

Lobov IB, Rao S, Carroll TJ, Vallance JE, Ito M, Ondr JK, Kurup S, Glass DA, Patel MS, Shu W, et al. (2005). WNT7b mediates macrophage-induced programmed cell death in patterning of the vasculature. Nature 437, 417–421. [PubMed: 16163358]

Lobov IB, Renard RA, Papadopoulos N, Gale NW, Thurston G, Yancopoulos GD, and Wiegand SJ (2007). Delta-like ligand 4 (Dll4) is induced by VEGF as a negative regulator of angiogenic sprouting. Proc. Natl. Acad. Sci. USA 104, 3219–3224. [PubMed: 17296940]

Lubarsky B, and Krasnow MA (2003). Tube morphogenesis: making and shaping biological tubes. Cell 112, 19–28. [PubMed: 12526790]

Maretto S, Cordenonsi M, Dupont S, Braghetta P, Broccoli V, Hassan AB, Volpin D, Bressan GM, and Piccolo S (2003). Mapping Wnt/beta-catenin signaling during mouse development and in colorectal tumors. Proc. Natl. Acad. Sci. USA 100, 3299–3304. [PubMed: 12626757]

Martin M, Potente M, Janssens V, Vertommen D, Twizere JC, Rider MH, Goris J, Dimmeler S, Kettmann R, and Dequiedt F (2008). Protein phosphatase 2A controls the activity of histone deacetylase 7 during T cell apoptosis and angiogenesis. Proc. Natl. Acad. Sci. USA 105, 4727–4732. [PubMed: 18339811]

Masckauchan TN, Shawber CJ, Funahashi Y, Li CM, and Kitajewski J (2005). Wnt/beta-catenin signaling induces proliferation, survival and interleukin-8 in human endothelial cells. Angiogenesis 8, 43–51. [PubMed: 16132617]

Masckauchan TN, Agalliu D, Vorontchikhina M, Ahn A, Parmalee NL, Li CM, Khoo A, Tycko B, Brown AM, and Kitajewski J (2006). Wnt5a signaling induces proliferation and survival of endothelial cells in vitro and expression of MMP-1 and Tie-2. Mol. Biol. Cell 17, 5163–5172. [PubMed: 17035633]

Minoguchi S, Taniguchi Y, Kato H, Okazaki T, Strobl LJ, Zimber-Strobl U, Bornkamm GW, and Honjo T (1997). RBP-L, a transcription factor related to RBP-Jkappa. Mol. Cell. Biol 17, 2679–2687. [PubMed: 9111338]

Morita K, Sasaki H, Furuse M, and Tsukita S (1999). Endothelial claudin. claudin-5/tmvcf constitutes tight junction strands in endothelial cells. J. Cell Biol 147, 185–194. [PubMed: 10508865]

Noseda M, Chang L, McLean G, Grim JE, Clurman BE, Smith LL, and Karsan A (2004). Notch activation induces endothelial cell cycle arrest and participates in contact inhibition: role of p21Cip1 repression. Mol. Cell. Biol 24, 8813–8822. [PubMed: 15456857]

Pirot P, van Grunsven LA, Marine JC, Huylebroeck D, and Bellefroid EJ (2004). Direct regulation of the Nrarp gene promoter by the Notch signaling pathway. Biochem. Biophys. Res. Commun 322, 526–534. [PubMed: 15325262]

Potente M, Urbich C, Sasaki K, Hofmann WK, Heeschen C, Aicher A, Kollipara R, DePinho RA, Zeiher AM, and Dimmeler S (2005). Involvement of Foxo transcription factors in angiogenesis and postnatal neovascula rization. J. Clin. Invest 115, 2382–2392. [PubMed: 16100571]

Potente M, Ghaeni L, Baldessari D, Mostoslavsky R, Rossig L, Dequiedt F, Haendeler J, Mione M, Dejana E, Alt FW, et al. (2007). SIRT1 controls endothelial angiogenic functions during vascular growth. Genes Dev. 21, 2644–2658. [PubMed: 17938244]

Rao S, Lobov IB, Vallance JE, Tsujikawa K, Shiojima I, Akunuru S, Walsh K, Benjamin LE, and Lang RA (2007). Obligatory participation of macrophages in an angiopoietin 2-mediated cell death switch. Development 134, 4449–4458. [PubMed: 18039971]

Ross DA, and Kadesch T (2001). The notch intracellular domain can function as a coactivator for LEF-1. Mol. Cell. Biol 21, 7537–7544. [PubMed: 11604490]

Shtutman M, Zhurinsky J, Simcha I, Albanese C, D'Amico M, Pestell R, and Ben-Ze'ev A (1999). The cyclin D1 gene is a target of the beta-catenin/LEF-1 pathway. Proc. Natl. Acad. Sci. USA 96, 5522–5527. [PubMed: 10318916]

Siekmann AF, and Lawson ND (2007). Notch signalling limits angiogenic cell behaviour in developing zebrafish arteries. Nature 445, 781–784. [PubMed: 17259972]

Srinivas S, Watanabe T, Lin CS, William CM, Tanabe Y, Jessell TM, and Costantini F (2001). Cre reporter strains produced by targeted insertion of EYFP and ECFP into the ROSA26 locus. BMC Dev. Biol 1, 4. [PubMed: 11299042]

Suchting S, Freitas C, le Noble F, Benedito R, Breant C, Duarte A, and Eichmann A (2007). The Notch ligand Delta-like 4 negatively regulates endothelial tip cell formation and vessel branching. Proc. Natl. Acad. Sci. USA 104, 3225–3230. [PubMed: 17296941]

Topczewska JM, Topczewski J, Szostak A, Solnica-Krezel L, and Hogan BL (2003). Developmentally regulated expression of two members of the Nrarp family in zebrafish. Gene Expr. Patterns 3, 169–171. [PubMed: 12711545]

Valenzuela DM, Murphy AJ, Frendewey D, Gale NW, Economides AN, Auerbach W, Poueymirou WT, Adams NC, Rojas J, Yasenchak J, et al. (2003). High-throughput engineering of the mouse genome coupled with high-resolution expression analysis. Nat. Biotechnol 21, 652–659. [PubMed: 12730667]

Veeman MT, Slusarski DC, Kaykas A, Louie SH, and Moon RT (2003). Zebrafish prickle, a modulator of noncanonical Wnt/Fz signaling, regulates gastrulation movements. Curr. Biol 13, 680–685. [PubMed: 12699626]

Xia CH, Liu H, Cheung D, Wang M, Cheng C, Du X, Chang B, Beutler B, and Gong X (2008). A model for familial exudative vitreoretinopathy caused by LPR5 mutations. Hum. Mol. Genet 17, 1605–1612. [PubMed: 18263894]

Xu Q, Wang Y, Dabdoub A, Smallwood PM, Williams J, Woods C, Kelley MW, Jiang L, Tasman W, Zhang K, et al. (2004). Vascular development in the retina and inner ear: control by Norrin and Frizzled-4, a high-affinity ligand-receptor pair. Cell 116, 883–895. [PubMed: 15035989]

Yun TJ, and Bevan MJ (2003). Notch-regulated ankyrin-repeat protein inhibits Notch1 signaling: multiple Notch1 signaling pathways involved in T cell development. J. Immunol 170, 5834–5841. [PubMed: 12794108]

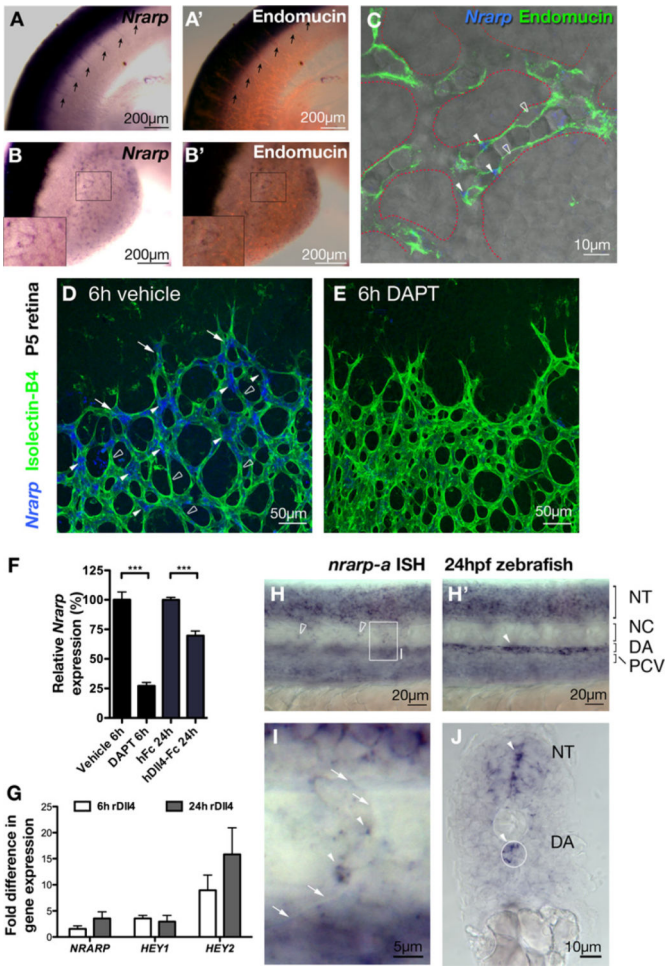

Figure 1. Endothelial *Nrarp* Expression Is Regulated by Notch Signaling

(A–C) In situ hybridization (ISH) of mouse *Nrarp* in mouse embryonic (E10.5) intersomitic vessels (arrows in [A]) and limb bud vessels ([B and C]; Endomucin, red). (C) Single plane confocal LSM image of limb bud vessels outlined with dotted red line (ISH reflection signal, blue; transmitted light; endomucin, green). *Nrarp* is more strongly expressed by ECs at branch points (filled arrowheads in [C]) compared to ECs in between (stroked arrowheads in [C]).

(D–G) Notch signaling positively regulates endothelial *Nrarp* expression. Whole-mount retina ISH shows high *Nrarp* expression (blue) in ECs (stained with Isolectin-B4, green) often located at vessel branch points in vehicle-treated P5 retinas (filled arrowheads, [D]) and absent in between branch points (stroked arrowheads). Endothelial stalk cells with *Nrarp* expression are indicated by arrows. Endothelial *Nrarp* expression decreased after 6 hr of DAPT treatment (E). (F) qPCR, relative expression of *Nrarp* in the retinas of P5 C57Bl6/J mice treated with DAPT (6 hr) or Dll4-Fc (24 hr). ***, $p \leq 0.0004$. Vehicle and DAPT treatments, $n \geq 7$; hFc, $n = 4$; Dll4-Fc, $n = 6$. Data show mean ± SEM, n = animals. (G) HUVECs were stimulated with rDll4 for 6 or 24 hr. Fold increase in *NRARP, HEY1* and *HEY2* expression are shown. $n = 3$.

(H–J) *nrarp-a* ISH in 24 hpf zebrafish embryos. (H) and (H′) are lateral views of the same region in the zebrafish trunk taken at different focal planes. The boxed region in (H) is

magnified in (I). (J) is a transverse section of the zebrafish trunk. *nrarp-a* is expressed in ECs of ISV (arrowhead, [I]) and in cells located between somite boundaries (empty arrowheads, [H]). *nrarp-a* is also expressed in the DA and in the neural tube (H′, J). Arrows in (I) indicate somite boundary. NT, neural tube; NC, notochord; DA, dorsal aorta; PCV, posterior cardinal vein.

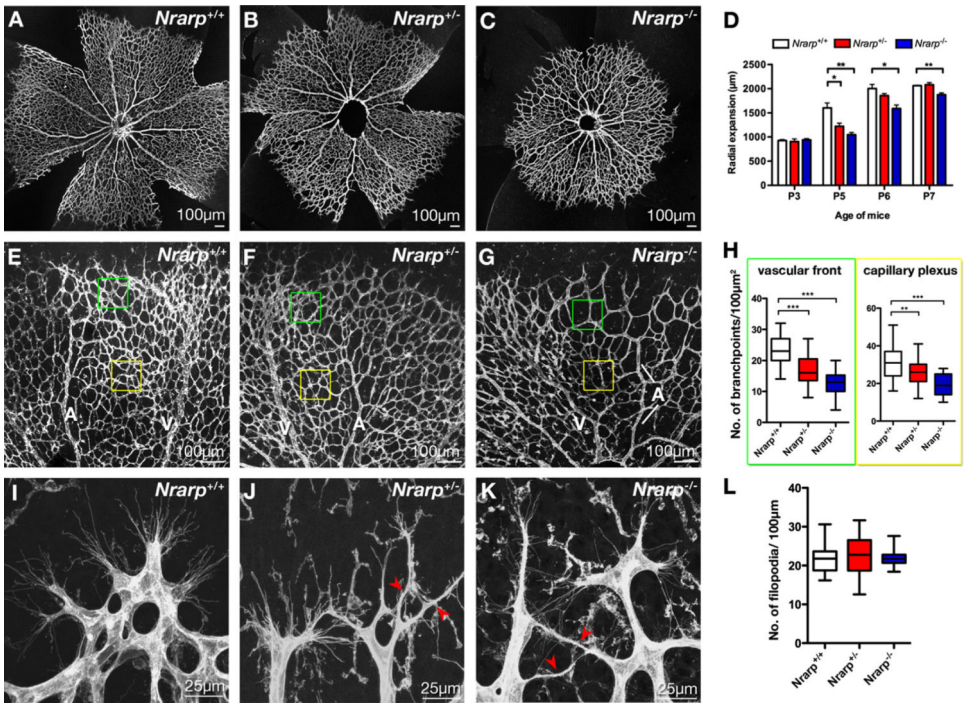

Figure 2. Loss of *Nrarp* Results in a Delay in Retinal Vascularization, a Decrease in Vessel Density, and Abnormal Vessel Morphology

(A–D) Gene dose-dependent delay in radial expansion of retinal blood vessel in *Nrarp*-deficient mice. Images of whole-mount P5 $Nrarp^{+/+}$, $Nrarp^{+/-}$, and $Nrarp^{-/-}$ retinas stained with collagen IV (A–C). (D) Bar graphs show mean distance of radial expansion (μm) ± SEM; **, $p < 0.01$; *, $p < 0.05$. $Nrarp^{+/+}$: P3, n = 8; P5, n = 6; P6, n = 3; P7, n = 3; $Nrarp^{+/-}$: P3, n = 5; P5, n = 15; P6, n = 12; P7, n = 4; $Nrarp^{-/-}$: P3, n = 4; P5, n = 4; P6, n = 4; P7, n = 5.

(E–H) Decreased vessel density in P5 *Nrarp* mutants. (E–G) Representative images of P5 $Nrarp^{+/+}$, $Nrarp^{+/-}$, and $Nrarp^{-/-}$ retinas stained with Isolectin-B4. Green and yellow boxes highlight the vascular front and capillary plexus, respectively, of retinal vessels analyzed for vessel density. Arteries (A); veins (V). (H) Quantification of vessel branch points/100 μm^2. ***, $p < 0.0001$; ** $p = 0.0079$. Vascular front: $Nrarp^{+/+}$, n = 21; $Nrarp^{+/-}$, n = 29; $Nrarp^{-/-}$, n = 18. Capillary plexus: $Nrarp^{+/+}$, n = 41; $Nrarp^{+/-}$, n = 30; $Nrarp^{-/-}$, n = 15.

(I–L) $Nrarp^{+/+}$, $Nrarp^{+/-}$, and $Nrarp^{-/-}$ retinas have similar number of filopodia protrusion. (I–K) Confocal images of tip cells stained with Isolectin-B4. Arrowheads indicate narrow vessels (J and K). (L) Quantification of filopodia/100 μm vessel length. $Nrarp^{+/+}$, n = 20; $Nrarp^{+/-}$, n = 23; $Nrarp^{-/-}$, n = 19. n = images.

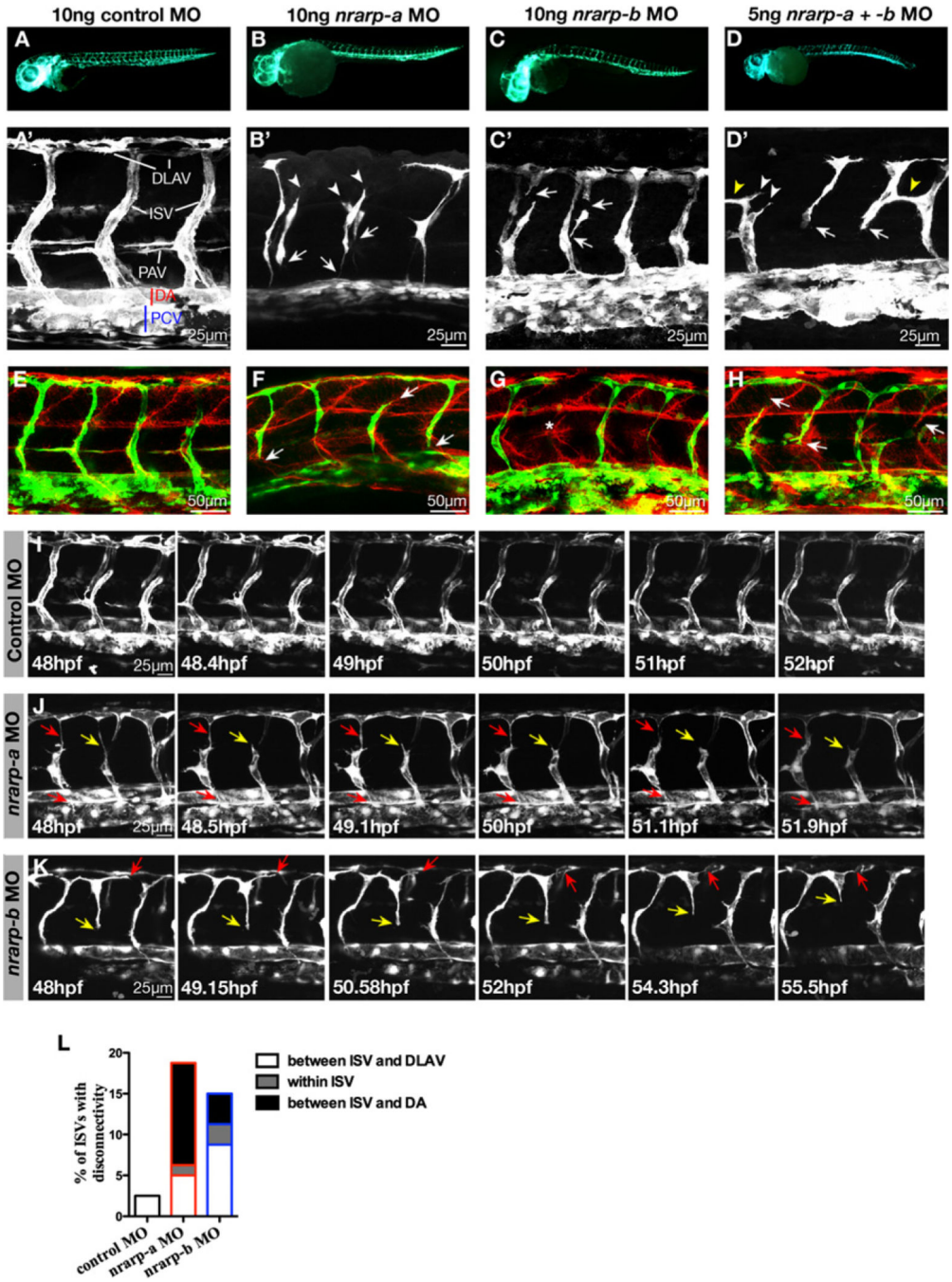

Figure 3. Knockdown of *nrarp-a* and *nrarp-b* in Zebrafish Leads to Abnormal Intersegmental Vessel Formation

(A–D) *Tg(fli1:EGFP)*^{y1} zebrafish were injected with 10 ng control (A), *nrarp-a* (B), *nrarp-b* (C), or 5 ng each of *nrarp-a* and *-b* (D) morpholinos and analyzed at ~56 hpf. (B′–D′) *nrarp-a* and *-b* morphants show defective ISVs. Arrows indicate disconnected vessels; arrowheads indicate ISVs with delayed dorsal migration; yellow arrowheads show misdirected ISV formation. Anterior of embryos is to the left. DLAV, dorsal longitudinal anastomotic vessel; ISV, intersegmental vessel; PAV, parachordal vessel; DA, dorsal aorta; PCV, posterior cardinal vein.

(E–H) Whole-mount collagen XII (red) staining in 48 hpf zebrafish *Tg(fli1:EGFP)*^{y1} embryos. Normal myotome boundaries are observed in *nrarp-a*, *-b*, and double *nrarp-a* and *–b* morphants (F–H). Arrows indicate disconnected vessels. * in (G) indicates missing ISV at the myotome boundary.

(I–K) Confocal time-lapse stills of control (I) and *nrarp-a* (J) or *nrarp-b* (K) morphants between 48 and 56 hpf. The ISVs of control morphants remained connected to the DA and DLAV (I). Note that the middle and right ISVs of the control morphant is out of focus. ISVs in *nrarp-a* and *-b* morphants regress over time (J and K). In (J), red arrows indicate poor connection between vessels and yellow arrow points to a regressing vessel. In (K), red arrow points to regressing vessel along the path of DLAV formation; yellow arrow indicates detachment of ISV from DA.

(L) Quantification of vessel disconnection. Graph shows the percentage of ISVs with disconnection between the ISV and DA, within the ISV, or between the ISV and DLAV. Ten embryos (8 ISVs/embryo) were analyzed for each morphant.

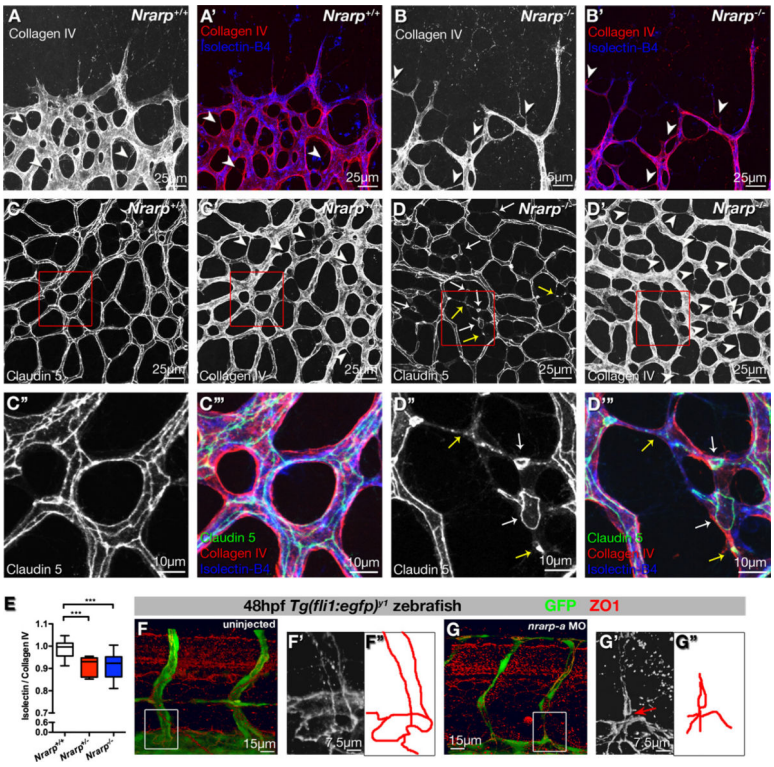

Figure 4. Loss of Nrarp Expression Causes Vessel Regression in Mouse and Zebrafish

(A and B) *Nrarp*$^{-/-}$ retinas display ectopic vessel regression at vascular front. P5 *Nrarp*$^{+/+}$ and *Nrarp*$^{-/-}$ retinas labeled for Isolectin-B4 (blue) and collagen IV (red). Arrowheads highlight empty collagen IV sleeves, indicating vessel regression.

(C and D) P6 *Nrarp*$^{+/+}$ and *Nrarp*$^{-/-}$ retinas labeled for Claudin 5 (green in [C″′ and D″′]), collagen IV (red in [C″′ and D″′]), and Isolectin-B4 (blue in [C″′ and D″′]). Increased vessel regression (arrowheads, [D′]) associates with discontinuous endothelial junctions in *Nrarp*$^{-/-}$ retinas (arrows, [D]). (D″) and (D″′) correspond to boxed regions in (D) and (D′). Yellow arrows indicate punctate Claudin 5 staining; white arrows point to loss of Claudin 5 continuity between vessels.

(E) Ratio of Isolectin-B4-positive vessels to collagen IV-positive vessels. Values below 1 indicate vessel regression. ***, $p < 0.0005$. *Nrarp*$^{+/+}$, n = 13; *Nrarp*$^{+/-}$, n = 8; *Nrarp*$^{-/-}$, n = 20.

(F and G) Zona occludens 1 (ZO1, red) staining in uninjected and *nrarp-a* MO-injected *Tg(fli1:EGFP)*^{y1} zebrafish embryos at 48 hpf. (F′) and (G′), high magnification Z-stacks of boxed regions in (F) and (G). Endothelial junctions (illustrated by red tracing) between the ISV and DA are poorly developed in *nrarp-a* morphants (arrow in [G′]).

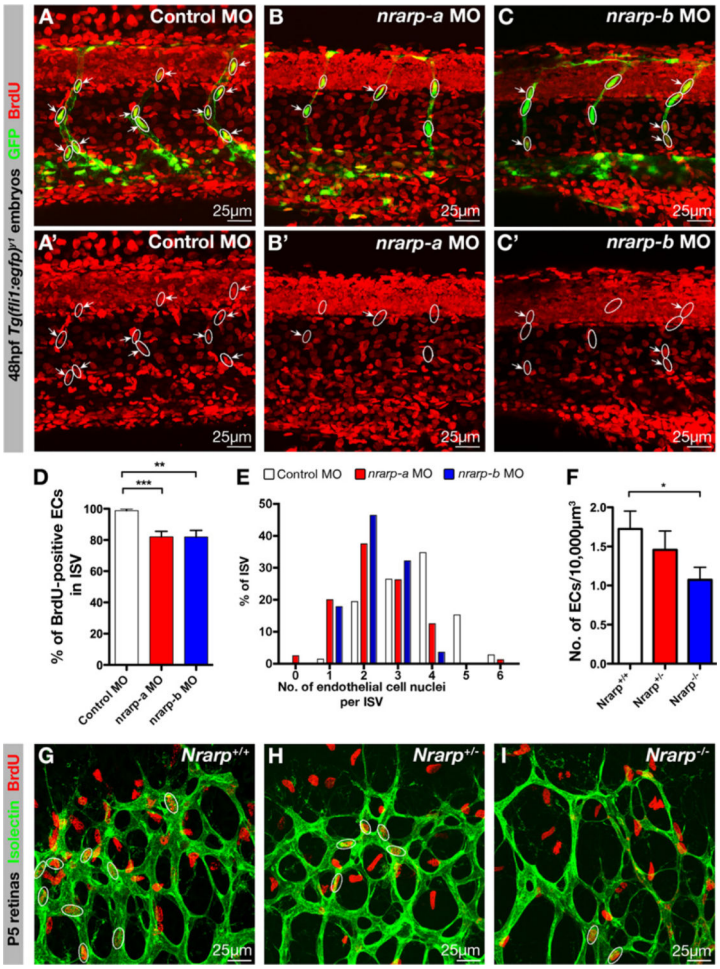

Figure 5. Decreased EC Proliferation in *Nrarp*$^{-/-}$ Mouse and in *nrarp-a* and *nrarp-b* Morphants

(A–D) Control, *nrarp-a* and *-b* MO-injected *Tg(fli1:EGFP)*^{y1} zebrafish embryos were exposed to BrdU (red) from 19 to 48 hpf. Circles highlight ECs nuclei along ISVs. Arrows indicate BrdU-positive ECs. (D) Quantification of BrdU-positive ECs in ISVs. Error bars indicate SEM. Control, n = 8 (31 ISVs); *nrarp-a*, n = 6 (47 ISVs); *nrarp-b*, n = 14 (66 ISVs). (E) Decrease in EC number in ISVs of *nrarp-a* and *-b* morphants. Bar graph shows the percentage of ISVs containing *x* number of endothelial nuclei per ISV at 48 hpf. Control MO, n = 17; *nrarp-a* MO, n = 16; *nrarp-b* MO, n = 21. Eight ISVs/embryo were analyzed. (F–I) 3 hr BrdU incorporation assay in P5 mice. Bar graph shows number of proliferated ECs in 10,000μm^3 retinal vessels (F). *, p = 0.0328. *Nrarp*$^{+/+}$, n = 17, *Nrarp*$^{+/-}$, n = 8; *Nrarp* $^{-/-}$, n = 14 images. Data show mean ± SEM. (G–I) Circles highlight BrdU-positive ECs in *Nrarp*$^{+/+}$, *Nrarp*$^{+/-}$, and *Nrarp*$^{-/-}$ retinas stained with Isolectin-B4 (green) and BrdU (red).

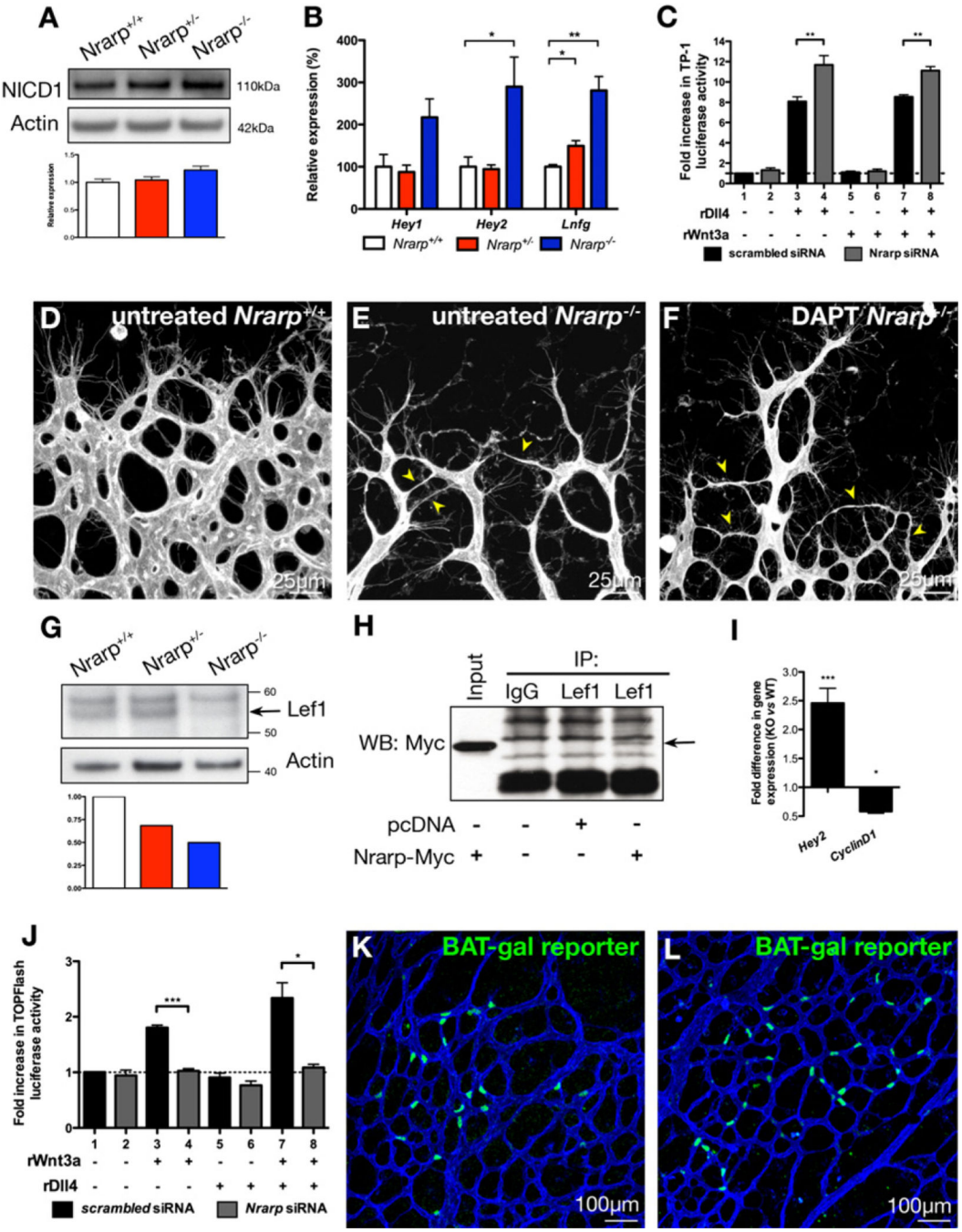

Figure 6. Loss of Nrarp Leads to Increased Notch Signaling and Reduced Wnt Signaling in ECs

(A) Western blot of Notch1 intracellular domain (NICD1) in P5 *Nrarp*$^{+/+}$, *Nrarp*$^{+/-}$, and *Nrarp*$^{-/-}$ retinas. n = 3 per genotype.

(B) qPCR of Notch target genes *Hey1*, *Hey2*, and *Lunatic fringe (Lnfg)* in P5 *Nrarp*$^{+/+}$, *Nrarp*$^{+/-}$, and *Nrarp*$^{-/-}$ retinas. **, $p < 0.01$; *, $p < 0.05$.

(C) TP-1 Notch reporter assay in HUVECs. HUVECs were stimulated with rDll4, rWnt3a, or both. **, $p < 0.01$. $n \geq 3$.

(D–F) Vascular front of P7 *Nrarp*$^{+/+}$, *Nrarp*$^{-/-}$, and DAPT-treated *Nrarp*$^{-/-}$ retinas stained with Isolectin-B4 (white). Arrows indicate thin and poorly connected vessels.
(G) Representative Western blot of Lef1 in P5 *Nrarp*$^{+/+}$, *Nrarp*$^{+/-}$, and *Nrarp*$^{-/-}$ retinas, densiometric analysis shown below blot.
(H) Coimmunoprecipitation experiment in HUVECs transfected with Nrarp-Myc. Endogenous LEF1 coimmunoprecipitates with Nrarp-Myc (arrow). Empty vector (pcDNA) was used as a control.
(I) Fold difference in expression (qPCR) of *Hey2* and *CyclinD1* in *Nrarp*$^{-/-}$ compared to *Nrarp*$^{+/+}$ ECs isolated from adult lungs. *, p = 0.019; ***, p = 0.0004. n = 6.
(J) TOPFlash Wnt reporter assay in HUVECs stimulated with Wnt3a and/or Dll4. *, p = 0.0014; ***, p = 0.0002. n = 3.
(K–L) BAT-gal reporter mouse shows Wnt activity (anti-β-galactosidase staining, green) in ECs of P4 retinal vasculature (Isolectin-B4, blue).
Error bars are ±SEM.

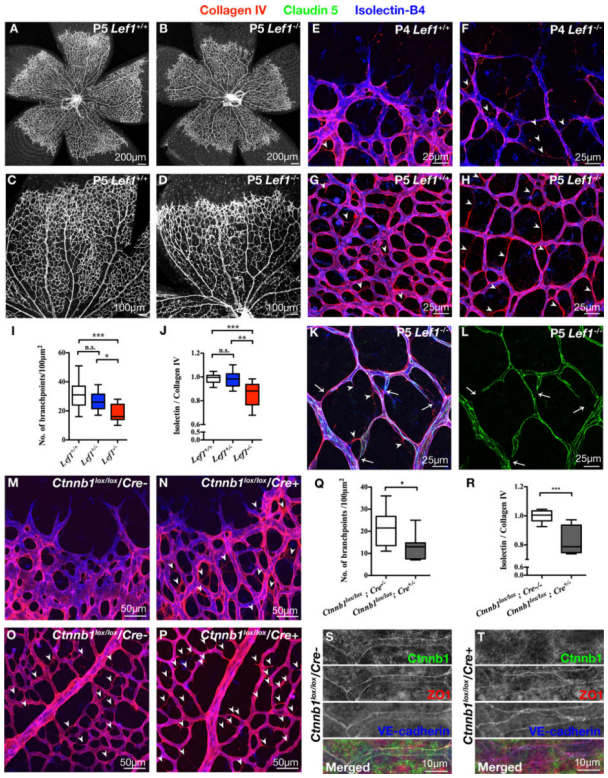

Figure 7. Loss of *Lef1* and Specific Endothelial Deletion of *Ctnnb1* Results in Decreased Vessel Density and Ectopic Vessel Regression

(A–D) P5 $Lef^{+/+}$ and $Lef1^{-/-}$ retinas stained with Isolectin-B4.

(E–H, K, and L) $Lef1^{-/-}$ retinas have increased empty collagen IV sleeves (red, arrowheads) at the vascular front (F) and in capillary plexus (H and K). Claudin 5 staining (green) reveals discontinuous endothelial junctions in $Lef1^{-/-}$. vasculature (arrows in [K and L]). Isolectin-B4, blue.

(I) Quantification of vessel branch points/100 μm^2 area in capillary plexus of $Lef1^{-/-}$ P5 retinas. *, p = 0.0150; ***, p < 0.0001. $Lef1^{+/+}$, n = 41; $Lef1^{+/-}$, n= 8; $Lef1^{-/-}$, n = 8.

(J) Quantification of vessel regression in the capillary plexus of $Lef1^{+/+}$, $Lef1^{+/-}$, and $Lef1^{-/-}$ P5 retinas. **, p = 0.048; ***, p = 0.0002. $Lef1^{+/+}$, n = 13; $Lef1^{+/-}$,n= 9; $Lef1^{-/-}$, n = 9.

(M–R) *Ctnnb1*$^{lox/lox}$; *Pdgfb-iCreER* mice, treated with tamoxifen at P4 and analyzed at P7. Inducible deletion of endothelial *Ctnnb1* resulted in increased empty collagen IV sleeves (arrowheads) at sprouting front (N) and in the plexus (P) when compared to control Cre negative littermates (M and O). Quantification of branch points/100 μm^2 (Q) and vessel regression (R) in the capillary plexuses of *Cre*-negative and *Cre*-positive littermates. *, p = 0.0279; ***, p = 0.0005. n ≥ 8.

. (S and T) Junctional localization of Ctnnb1 (green), ZO-1 (red), and VE-cadherin (blue) in retinal capillaries. Junctional ZO-1 and VE-cadherin are retained despite complete loss of junctional Ctnnb1 in *Ctnnb1*$^{lox/lox}$; *Pdgfb-iCreER* mice (T).